Front. Earth Sci. 2022, 16(2): 483–498
https://doi.org/10.1007/s11707-022-0990-5

RESEARCH ARTICLE

# Multi-scale fractures formation and distribution in tight sandstones—a case study of Triassic Chang 8 Member in the southwestern Ordos Basin

**Gaojian XIAO[1], Ling HU[2], Yang LUO (✉)[1], Yujing MENG[1], Ali Bassam Taher AL-SALAFI[3], Haoran LIU[4]**

1 Key Laboratory of Tectonics and Petroleum Resources, China University of Geosciences, Wuhan 430074, China
2 Wenhua College, Wuhan 430074, China
3 Faculty of Petroleum and Natural Resources, Sana'a University, Sana'a, Yemen
4 Louisiana State University, Baton Rouge LA 7080, USA



**Abstract** Fracture system is an important factor controlling tight oil accumulation in the Triassic Chang 8 Member, southwestern Ordos Basin, China. A systematic characterization of the multi-scale natural fractures is a basis for the efficient tight oil production. Based on outcrops, seismic reflections, well cores, well logs (image and conventional logging), casting thin sections, and scanning electron microscope observation, the multi-scale fractures occurrences and their influences on Chang 8 tight sandstone reservoirs are revealed. The results show that three periods of strike-slip faults and four scales of natural fractures developed, namely mega-scale (length > $7 \times 10^7$ mm), macro-scale ($3.5 \times 10^5$ < length < $7 \times 10^7$ mm), meso-scale (10 < length < $3.5 \times 10^5$ mm), and micro-scale (length < 10 mm) fractures. The mega- and macro-scale fractures developed by strike-slip faults are characterized by strike-segmentation and lateral zonation, which connect the source and reservoir. These scale fractures also influence the distribution and effectiveness of traps and reservoirs, which directly influence the hydrocarbon charging and distribution. The meso fractures include the tectonic, diagenetic, as well as hydrocarbon generation-related overpressure types. The meso- and micro-scale fractures improve the sandstone physical properties and also the tight oil well production performance. This integrated study helps to understand the distribution of multi-scale fractures in tight sandstones and provides a referable case and workflow for multi-scale fracture evaluation.

**Keywords** natural fractures characteristics, geological significance, tight sandstone reservoir, Upper Triassic Yanchang Formation

Received September 16, 2021; accepted March 16, 2022

E-mail: luoyang0802@163.com

## 1 Introduction

A natural fracture system is an important factor to control the physical properties, migration, accumulation of hydrocarbons, and distribution of "sweet spot" in tight sandstone reservoirs (Wang et al., 2010; Zou et al., 2013). Over the last two decades, the viewpoint of "no fractures, no hydrocarbon accumulation" has been put forward based on the practical exploration and development of fractured tight sandstone reservoirs (Dai and He, 2010; Zeng et al., 2013). Therefore, the characterization and evaluation of natural fractures in tight sandstones have always been a research priority area.

Many studies on natural fracture characterization and evaluation have been conducted from different perspectives: the development pattern of natural fractures was quantitatively analyzed in three dimensions by imaging well logs (Pan et al., 2010). The characteristics of fractures in the Mesozoic stratums of the Ordos Basin were summarized, in which six sets of fractures are divided into three periods, and their controlling factors are analyzed (Jiang et al., 2013). Olson et al. (2009) ulteriorly expounded the underlying mechanisms and diagenesis responsible for the development of fractures. The characteristics of natural fractures and their mechanics controlling factors are analyzed in tight sandstones (Baytok and Pranter, 2013). The finite element method based on geomechanical models is used to analyze the developmental characteristics of tectonic fractures in the Ordos Basin (Ju, 2020)

Seismic interpretation can provide continuous stratigraphic information to extract natural fractures, many

constraints limit the use of seismic data (Derikvand et al., 2019). However, the resolution of seismic data often leads to ignoring many natural fractures. Most of the studies have performed fracture response analysis from a single or multiple log series, and little thought has been given to the characterization and pre-processing of fracture log response data.

Previous studies mainly focus on fractures as a factor affecting reservoir quality and favored fractures of single genesis or scale, lacking accurate delineation of complex fractures system and systematic discussion of the hydrocarbon geological significance of natural fractures of different genesis and scales (Bai et al., 2012; Han et al., 2021; Luo et al., 2021). Therefore, the existing characterizations cannot elucidate the development patterns of multi-scale fractures. A comprehensive evaluation and characterization of multi-scale fractures using multi-scale data must be essential for the understanding of the formation mechanism, main controlling factors, and distribution of "sweet spots" in tight sandstones.

The Honghe Oilfield is located in the northwest Ordos Basin, China. The Upper Triassic Yanchang Formation of the Honghe oilfield has been proven to be resource potential tremendous (Zou et al., 2013). The Yanchang tight sandstones have undergone strong diagenesis, resulting in complex pore-throat structures and loss of primary pores, and therefore highly heterogeneous (Wang et al., 2017c; Yao et al., 2018).

However, it shows a good correlation with the distribution of "sweet spot" reservoirs for the multi-scale fracture system due to their positive effects on hydrocarbon accumulation, formation of reservoirs, trap, and high productivity. Exploration and development practice shows that the distribution of the "sweet spot" in Chang 8 tight sandstones is always closely related to the multi-scale fracture zones controlled by multi-scale strike-slip fault band (Zeng et al., 2013). The multi-scale natural fractures span greatly, ranging from kilometers to micrometers, which makes difference in petroleum geological significance and evaluation approaches. In general, mega–macro scale fracture systems are generally analyzed using approaches such as field outcrops (to determine the type of fracture system), seismic interpretation combined with well logs (to determine the scale and boundary of fracture system), and the regional tectonic stress field simulation (to determine the structure of the fracture zone), while meso and micro-scale fractures are generally characterized by core and casting thin sections, SEM images, and micro CT analysis. Therefore, a comprehensive evaluation and characterization of multi-scale fractures using multi-scale approaches are essential for the understanding of the formation mechanism, main controlling factors, and distribution pattern of "sweet spots".

In this paper, multi-scale data, such as field outcrops, cores, logging (conventional logging and images well logging), casting thin sections, and scanning electron microscope images, are used to describe the characteristics of multi-scale natural fractures system, and combining carbon/oxygen isotopes and fluid inclusion data, the different petroleum geological significance of multi-scale fractures in controlling hydrocarbon accumulation, development of reservoirs and trap, physical properties (porosity and permeability), and high productivity and production were analyzed.

## 2 Geological setting

The study area, Honghe Oilfield, is located in south-west of the Ordos Basin (Fig. 1), which occupies an area of approximately 2500 km$^2$. The fault and fracture systems in the study area are mainly caused by Liupanshan thrust nappe and Qinling thrust nappe (Zeng et al., 2010b; Deng et al., 2013). The main tectonic movement that has had a primary influence on the development and distribution of multi-scale fractures in the Chang 8 tight sandstones are the Yanshanian Tectonic Movement from the Middle Jurassic to late Early Cretaceous and the Himalayan Tectonic Movement occurred in the Cenozoic, which combined have a significant influence on the geomorphologic structure feature of the Yanchang sandstones.

Previous research has proven that the main oil-bearing formation mainly developed in the Mesozoic sedimentary strata (Duan et al., 2008; Zhang et al., 2015). The study concentrates on the Upper Triassic Yanchang Formation, which stratum in the Honghe area is a set of sandstones deposited in the braided delta front (Wang et al., 2017b; Yao et al., 2018). The Upper Triassic Yanchang Formation has composed of Chang 10 to Chang 1 Oil Member from the bottom to the top (Fig. 2). The main composition of the Chang 8 stratum is an upward coarsening sedimentary sequence.

## 3 Methodology

### 3.1 Methods

The data for multi-scale fracture characterization need to cover different resolutions (μm–km). The field outcrops can be used for systematic observation and description of mega-scale fracture systems, and seismic profile data are used to analyze mega-scale fractures, whose resolution in vertical and lateral directions are 50 m and 300 m respectively. The vertical and lateral resolutions of the well logging are 0.125 m and 1 m, respectively, thus allowing the description of macro-scale fractures at the meter level. The core data have a naked-eye level resolution, which can be used for the description at the centimeter level. Casting thin sections and scanning electron microscope (SMI) images have millimeter and micron-level resolutions, thus allowing the description of fractures at the micro-scale. For the characterization of mega-scale fracture systems, the development pattern and

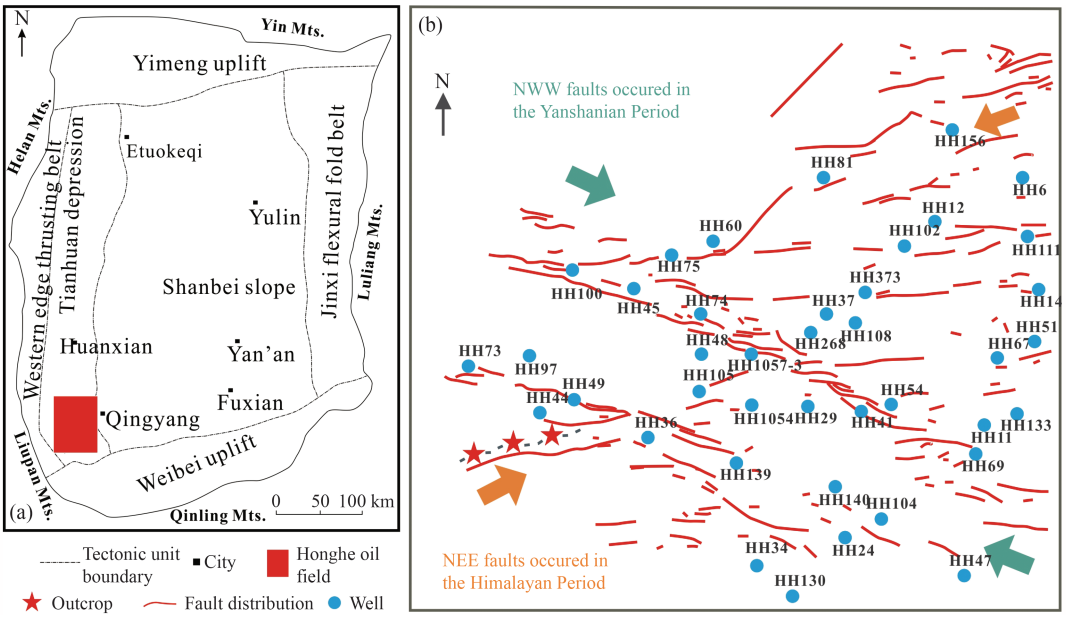


**Fig. 1** Structural division map of the study area, outcrops, wells, and fault distribution in the Ordos Basin. (a) Location of the Honghe oilfield and tectonic units of the Ordos Basin. (b) Distribution of faults, outcrops, and wells in the Chang 8 layer of the Honghe Oilfield.

| Formation | Member | Sub-Member | Thickness /m | Lithology | Sedimentary Facies |
|---|---|---|---|---|---|
| Upper Triassic Yanchang Formation | Ch1 | $Ch1_1$ | 0–240 | | Meande ring river |
| | | $Ch1_2$ | | | |
| | | $Ch1_3$ | | | |
| | Ch2 | $Ch2_1$ | 120–150 | | Braided river |
| | | $Ch2_2$ | | | |
| | | $Ch2_3$ | | | |
| | Ch3 | $Ch3_1$ | 90–110 | | Meande ring river |
| | | $Ch3_2$ | | | |
| | | $Ch3_3$ | | | |
| | Ch4+5 | $Ch4+5_1$ | 80–90 | | |
| | | $Ch4+5_2$ | | | |
| | Ch6 | $Ch6_1$ | 110–130 | | |
| | | $Ch6_2$ | | | |
| | | $Ch6_3$ | | | |
| | Ch7 | $Ch7_1$ | 100–120 | | Delta |
| | | $Ch7_2$ | | | |
| | | $Ch7_3$ | | | Lake |
| | Ch8 | $Ch8_1$ | 80–100 | | Braided river |
| | | $Ch8_2$ | | | |
| | Ch9 | $Ch9_1$ | 80–100 | | Delta |
| | | $Ch9_2$ | | | Lake |
| | Ch10 | $Ch10_1$ | 210–350 | | Delta |
| | | $Ch10_2$ | | | Braided river |
| | | $Ch10_3$ | | | |

Oil shale Mudstone Coarse grained sandstone
Medium grained stone Fine grained stone

**Fig. 2** The composite stratigraphic columns of the Triassic Yanchang Formation in the Ordos Basin (Ch represents Chang).

the statistical relationship between fractures and faults can be determined by outcrop observation. The interpretation of seismic profile by a combination of well logs and seismic can be used to determine fractures in the mega-scale, and seismic attributes and inversions can be used to delineate the boundaries of the fracture system (Li et al., 2016, 2019a, 2019b).

For characterization of macro-scale fracture system, well logging is used to identify and predict distribution pattern of fracture. The combination of imaging log analysis and seismic ant attribute analysis can be used to analyze the distribution characteristics of fractures in three-dimensional. Meso-scale fracture characterization mainly relies on core description to observe and record fracture type, intensity, and other distribution features, analyze the main controlling factors of fracture development, and calculate evaluation parameters (porosity and permeability of meso-scale fractures). Micro-scale fracture characterization is mainly based on the observation of fracture size, openness, combination relationship, cementation, and shows of hydrocarbon in thin section and SMI images, and then analyze the fracture development period and control characteristics in reservoirs. Based on the characterization of fractures at different scales, the carbon and oxygen isotope analysis and fluid inclusion techniques are used to analyze the evolution of multi-scale fractures and the geological significance of multi-scale fractures in tight sandstones. Finally, we establish a "sweet spots" model and provide a basis for the exploration and development of tight fractured sandstone reservoirs.

## 3.2 Data

3D seismic data volume of 2533.6 $km^2$ in the Honghe

Oilfield has been collected, and 30 km$^2$ is used for the characterization of the mega-scale fractures and the features of regional geological structure. The Nashuihe outcrop is located in south-west of the study area (Fig. 1), whose geological reconnaissance of outcrops observation extends for about 4 km.

Five Full-bore Microscan Images (FMI) well logs and 40 conventional well logs are selected for evaluating characteristics of natural fractures, including 9 petrophysical logs, namely Gamma-Ray log (GR), Spontaneous Potential log (SP), Dual Caliper (CAL), Acoustic log (AC), Bulk Density log (DEN), Compensated Neutron Porosity log (CNL), Deep Induction log (ILD), Middle Induction log (ILM), and Laterolog-8 (LL8).

Fracture observation and description of cores, including the types of the micro-fractures (tectonic, diagenetic, and overpressure-related fractures), scale (length and aperture), orientation, dip angle, filling degree, oil-bearing degree, were conducted for 2067.5m of cores from 40 wells. Meanwhile, fracture dip angles, length, and apertures are recorded. The correction between aperture under-layer and that on the earth's surface was conducted by the coefficient of apertures and hydrostatic confining stresses (Zeng et al., 2010a).

320 casting thin sections and 176 Scanning Electron Microscope (SEM) images were used to analyze the types, characteristics, and richness of micro-scale fractures. Apertures were recorded and calculated by the empirical relationship between apertures and hydrostatic pressure, whose morphology and origin are analyzed, and the fractures developing environment were also briefly discussed. For casting thin section observations, tight sandstone samples were pressurized to 6–7 MPa at room temperature (24°C), and red resin was injected into the oil-free sample, then dried at 100°C and held for two hours. The microfractures are filled with red resin in thin sections, whose observation instrument for microfractures was an Olympus polarizing microscope, at room temperature and the humidity was 35%. The analytical instrument for SEM image observation was a Phenom ProX system, using experimental voltages of 220V under vacuum.

The formation time of fractures are deduced from the values of $\delta^{18}O_{PDB}$(‰) and $\delta^{13}C_{PDB}$(‰) of calcite-cement filled in the fractures. 13 mineral samples filled in fractures in tight sandstones from Nashuihe outcrops are collected for isotopes of carbon/oxygen experiment. Fractures are mainly filled by calcite, which is primarily endowed in high dip angle or vertical fractures. Meanwhile, the hydrocarbon charging period can be deduced by calculating the homogenization temperature of fluid inclusions. The analytical instrument for fluid inclusions observation was an Olympus polarizing microscope, and the THMSG600 hot and cold worktop is used to conduct microscopic temperature measurements with a precision of ±0.1°C.

## 4 Description and characterization of multi-scale fractures

### 4.1 Mega-scale fracture system

According to the seismic interpretation of the Chang 8 Member of the Honghe Oilfield, three scales and three periods of tectonic movements of strike-slip faults and associated fracture systems are found (Fig. 3). Mega and

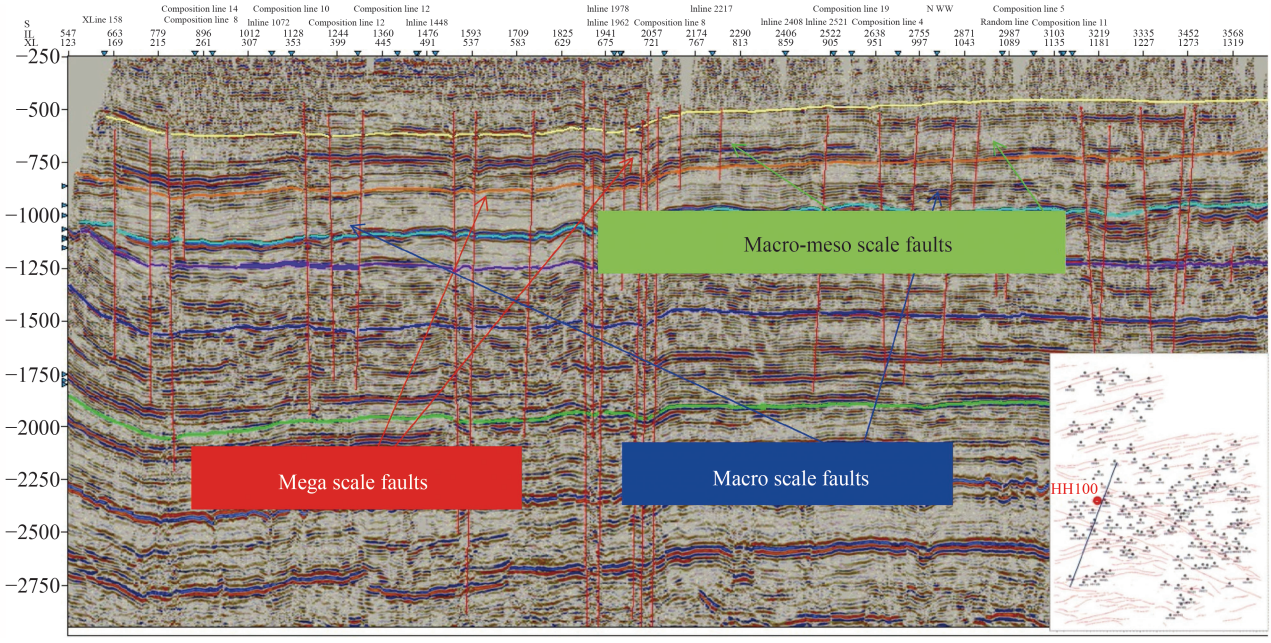


**Fig. 3** Different scales strike-slip faults in 3 periods of the Honghe Oilfield on seismic profile.

macro-scale fracture zones and meso-scale (intra-formation) fracture zones, which developed during the Indochina, Yanshannian, and Himalayan Periods, respectively. Three groups of strike-slip fault bands (NW, NE, and NEE) can be distinguished on the plane (Fig. 1(c)), among which, NW and NEE strike-slip faults are the most developed (Fig. 3).

The NW strike Yudu fault-fractured band is a mega-scale strike-slip fault-fracture system in the Honghe Oilfield, with a length of greater than 7000 m, an upright fault surface, an obvious break of the seismic horizons, and fault displacement greater than 50 m, which represents strong fault movement. It longitudinally cut through the Cretaceous, the Triassic and upward extension to the overlying shallow strata, reflecting the emergence of the faults in the Middle to Late Triassic, where there are multi-episodes tectonic movements in the later stages.

The Nashuihe outcrop is located on the Yudu fault-fractured band, which is the part of basin extension of the Haiyuan fault-fractured band developed at the combination between the Qinghai-Tibetan plate and the western boundary of the basin, which extends to the south to the Weibei Uplift in the Jinghe area (Fig. 3). Outcrop descriptions indicate that the Yudu fault-fractured band is mainly associated with four groups of fractures (NNW, NNE, NE, and EW), with NE and NW fractures dominating, and NE fractures limiting EW fractures (Fig. 4), representing mega-scale shear fractures associated with Yanshanian (sinistral) and Xishanian (Dextral) tectonic movement, respectively.

### 4.2 Macro scale fractures system

The macro-scale fractures correspond to NEE strike-slip fault-fractures bands (length > 3500 m, high angle, displacement > 10 m) developed in the middle Jurassic Yanshannian Period. The macro-scale slip fault-fractures are dextral strike-slip derivatives of the Yudu fault-fractured belt, mostly arranged in rows or en-echelon. They are often accompanied by NNE tensor upright joints (tension-type) and NW and NE high-angle shear joints derived from the dextral strike-slip in the Himalayan period.

In FMI logs interpretations, the open vertical and inclined fractures presented as dark traces with mud filtrate invasion (Fig. 5). 5 FMI wells interpretation indicated that two main combinations of fractures exist in the Chang 8 tight sandstones, with NE-SW and NW-SE in the strike (Fig. 4(b)). Three porosity logging suites can be used to determine the presence of fractures, which result in increased AC, DEN, and CNL values (Table 1, Fig. 5).

The combination of ILD, ILM, and LL8, in this paper, is used to analyze the effect of fractures. The change of the ILD and ILM curves can reflect the resistivity of the uninvaded zone and the invaded zone, respectively, while the LL8 curves can reflect the resistivity of the flushed zone.

In this paper, the fractures can be determined by comparing the ILD, ILM, and LL8 curves in Chang 8 tight sandstones (Table 1). The response characteristics of conventional logs to fractures are compared according to the intensity of the linear fracture (> 1.75/m and < 0.45/m) based on the results of the core description and the imaging well logs interpretation (Fig. 5). In the wells with fractures intensity greater than 1.75/m, the fractures response of Dual caliper, AC, DEN, CNL, ILD, ILM, and LL8 have quite a distinction between fractured and unfractured layers. Nevertheless, in the wells with fractures intensity less than 0.45/m, the fractures response of CAL, AC, DEN, CNL, ILD, ILM, and LL8 are relatively lacking significant differentiation for fractures identification.

### 4.3 Meso-scale fractures system

#### 4.3.1 Meso-scale fractures on cores

The meso-scale fractures system mainly developed during the Himalayan period, which includes small normal faults with complex strike and transform faults modified by the

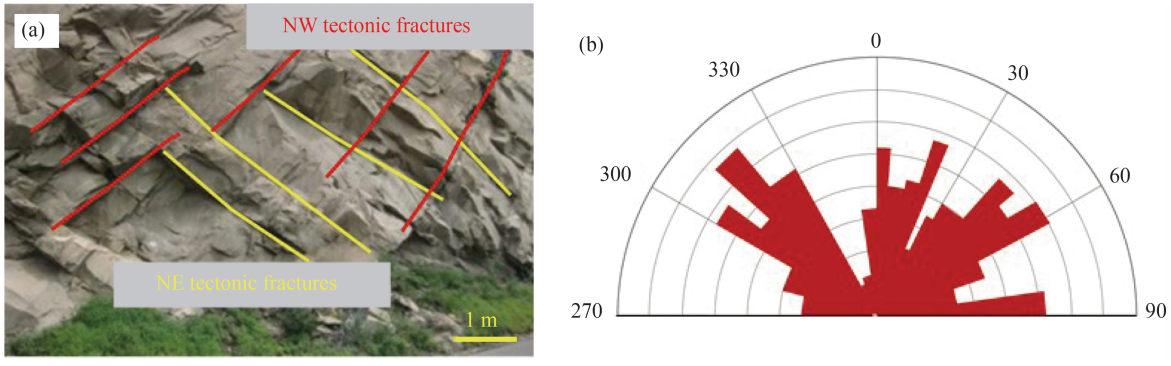


**Fig. 4** Photos of fractures exposed in the Nashuihe outcrops. (a) Fractures with NW and NE trending in gray fine sandstones were 2–9 m in length and present scratches on the surface. (b) Rose diagram of fracture strikes from Nashuihe outcrops ($N$ = 985, photos, and data from the China North Branch of Sinopec, collected by Zeng LB).

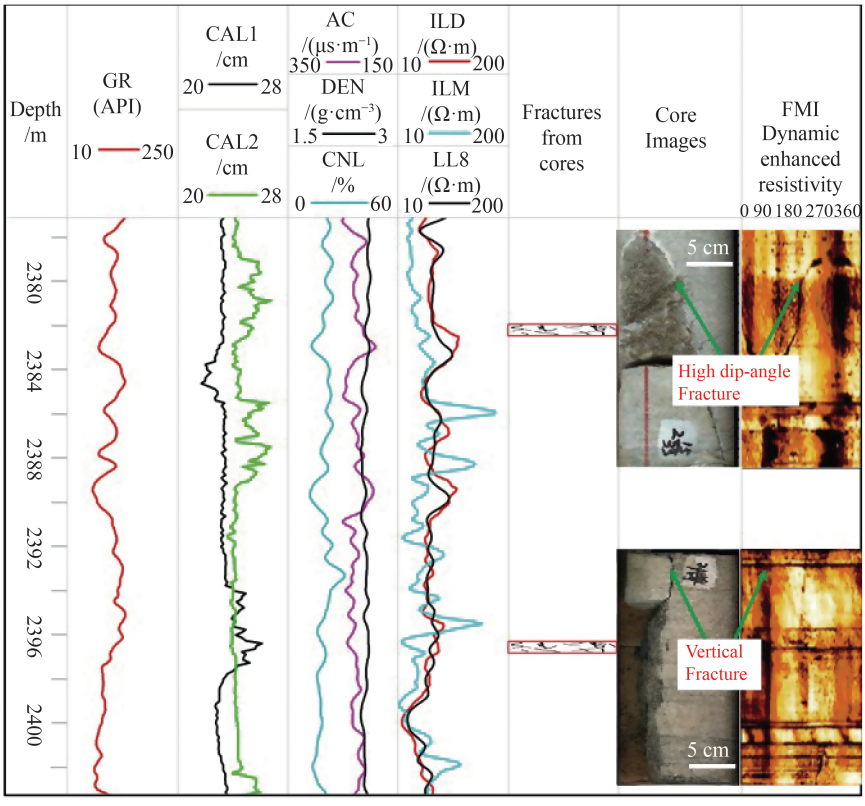


**Fig. 5** Response characteristics of natural fractures in the HH90 Well of the Chang 8 layer. In the track of Full-bore Microscan Images (FMI) and core images, the arrows show fractures with high dip-angle and nearly 90°.

**Table 1** Fracture response characteristics of conventional well logs in Chang8 tight sandstones

| | Wells (fractures intensity <0.5/m) | | Wells (fractures intensity >1.75/m) | | |
|---|---|---|---|---|---|
| | Fractured layers | Unfractured layers | Fractured layers | Unfractured layers | Only correspond to fractures |
| CAL1(cm) | 20.62–27.71 | 20.61–26.53 | 20.58–27.74 | 20.2–23.98 | 23.98–27.74 |
| CAL2(cm) | 21.31–27.05 | 21.31–26.71 | 19.09–31.22 | 18.68–24.31 | 24.31–31.22 |
| AC(μs/m) | 191.58–270.19 | 189.82–271.83 | 193.94–280.39 | 185.75–243.95 | 185.75–280.39 |
| DEN(g/cm$^3$) | 2.3–2.68 | 2.3–2.66 | 2.18–2.65 | 2.19–2.68 | 2.19–2.65 |
| CNL(%) | 9.23–29.29 | 9.74–27.43 | 8.94–36.75 | 6.87–28.65 | 28.65–36.75 |
| ILD(Ω•m) | 2.96–62.98 | 4.11–63.11 | 6.24–58.29 | 13.35–73.15 | 6.24–13.35 |
| ILM(Ω•m) | 3.52–68.73 | 5.25–60.01 | 7.94–68.89 | 20.96–92.92 | 7.94–20.96 |
| LL8(Ω•m) | 2.78–111.71 | 5.78–94.86 | 5.77–99.54 | 19.04–133.73 | 5.77–19.04 |

Himalayan tectonic movement (extension length less than 3500 m, high dip angle, displacement less than 10 m). Cores are mainly used for the characterization of meso-scale fractures. According to the core observations, fractures in the Chang 8 tight sandstones can be mainly divided into three types (tectonic, diagenesis, and overpressure-related fractures), with tectonic fractures dominant (Fig. 6).

#### 4.3.1.1 Tectonic fractures

Most fractures in the Chang 8 layer result from the variations of local tectonic movements and tectonic stress fields (Jiang et al., 2013; Wei et al., 2020). The evaluation indicators of tectonic fracture system mainly consist of fracture dip angle, morphology, strike, etc (Nelson et al., 2000), they not only affect the flow performance of fluids but also affect fracture permeability and the response characteristics of fractures to well logs (Dai et al., 2010; Liu et al., 2013).

Based on the fracture dip angle, the tectonic fractures in this paper can be classified into 4 types: low dip-angle (< 30°) (Fig. 6(a)), middle dip-angle (30°–60°) (Fig. 6(b)), high dip-angle (60°–80°) and vertical tectonic fractures (Figs. 6(c)– 6(f)). Based on the mechanical origin, their structures can be divided into fractures under tensile

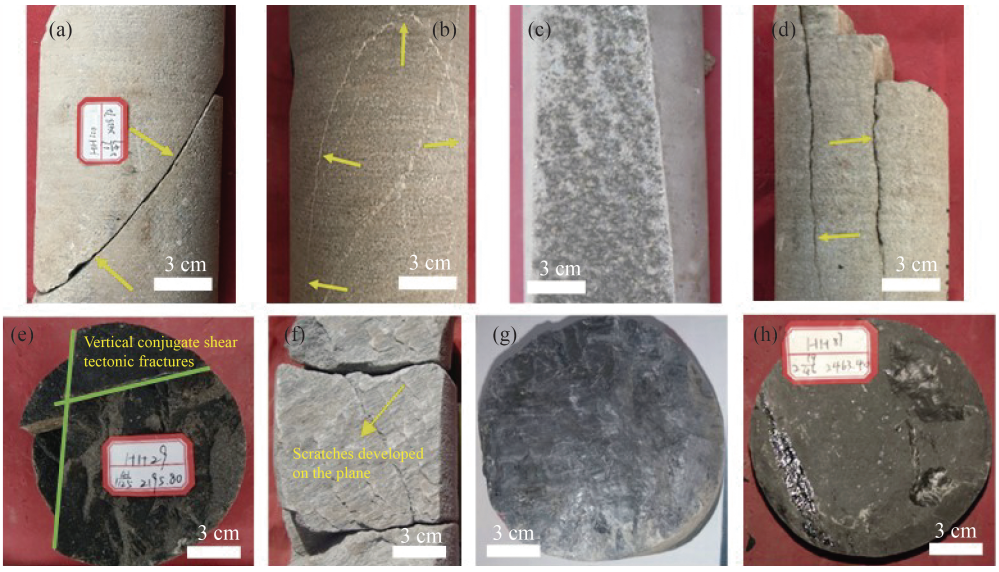


**Fig. 6** Pictures of different types of fractures. (a) HH100 well, 2428.72 m, fine sandstones, showing high dip-angle tectonic shear fractures (yellow arrow) without filling. (b) HH87 well, 2462.48 m, dark gray sandstone, showing high dip-angle fractures (yellow arrow) filled with calcite. (c) HH158 well, 2142.67 m, fine sandstones, showing vertical shear fractures with the oil patch. (d) HH1057-3 well, 2229.61 m, gray fine sandstones, showing two parallel vertical overpressure-related fractures. (e) HH29 well, 2195.81 m, brown muddy siltstone, showing a set of vertical conjugate tectonic fractures (yellow arrow). (f) HH42 well, 1784.50 m, showing conjugate scratches. (g) ZJ4 well, 2049.9 m, dark gray silty mudstone, showing diagenetic fracture. (h) HH87 well, 2463.40 m, dark brown silty mudstone, showing horizontal shrinkage fractures filled with bitumen.

stress (Figs. 6(d) and 6(f)) and shear stress (Figs. 6(a), 6(b), and 6(e)). Extensional fractures generally showed as rough and irregular in fractures planes, whose extended lengths are limited (Figs. 6(e) and 6(f)). High dip-angle and vertical tectonic fractures are predominantly shear fractures, which are characterized as smooth in fractures planes, straight fractures lines.

From core observations, tectonic fractures are dominated by high dip-angle fractures (Fig. 7(a)), most of which are vertical (54.71%). The development of low and middle dip-angle tectonic fractures is weak (21.37% and 23.92%), and they are mainly sorted in mudstones (Fig. 7(b)). The orientation of fracture is controlled by lithology. Most of the high dip-angle fractures (80–90) mainly emerged from fine sandstones (Fig. 7(b)), which are accounted for 43.75% of the total and twice or even more than in siltstone and muddy siltstone. The proportions of inclined fractures in muddy stone and silty mudstone are close to approximately 20%.

The length of fractures (83.18%) in cores ranges from 10 cm to 100 cm, with dominated being 10–20 cm (Fig. 7(c)). The frequency of less than 5% mainly focused on the intervals of fractures length less than 10 cm and larger than 60 cm. These fractures cut through thin sandstone and mudstone layers and show a good connecting effect longitudinally.

The distribution of fractures width has been rather dispersed and the intervals of 200–300 μm, 400–500 μm, and 900–1000 μm are relatively concentrated with respectively 12.94%, 14.56%, and 17.80% (Fig. 7(d)). The fractures fillers with a width less than 100 μm mainly developed in mudstone and muddy sandstones and apertures in the mudstone are generally less than that in sandstones.

The fracture filler in sandstones is dominated by quartz and calcite cement, with a small amount of muddy cement. The filling rates are high overall, and the effectiveness in sandstones with noncalcareous cementation is better than that with calcareous cementation. In sandstones with noncalcareous cementation, the proportion of unfilled is 45.78% (Fig. 8(a)), fully filled is 34.51%, half-filled is 11.15%, and partly filled is 8.56%, which belongs to the higher middle level of the effectiveness. However, fractures in sandstones with noncalcareous cementation present worse effectiveness with 55.65% filled (Fig. 8(b)).

#### 4.3.1.2 Diagenetic fractures

Diagenetic fractures developed under volume expansion like quartz secondary enlargement expelled fluid from compaction, and pressure solution (Ding et al., 2013), which mainly developed in the silty mudstone and mudstone with patterns of fold-shaped parallel to the bedding structures (Figs. 6(g) and 6(h)). The crystal structure of clay minerals, like smectite, changed with the progress of turning into illite and chlorite, which causes contraction accompanied by a decrease of partial argillaceous sandstones volume and primarily occurs during the middle and advanced stage.

#### 4.3.1.3 Overpressure-related fractures

Overpressure-related fractures in cores are mainly

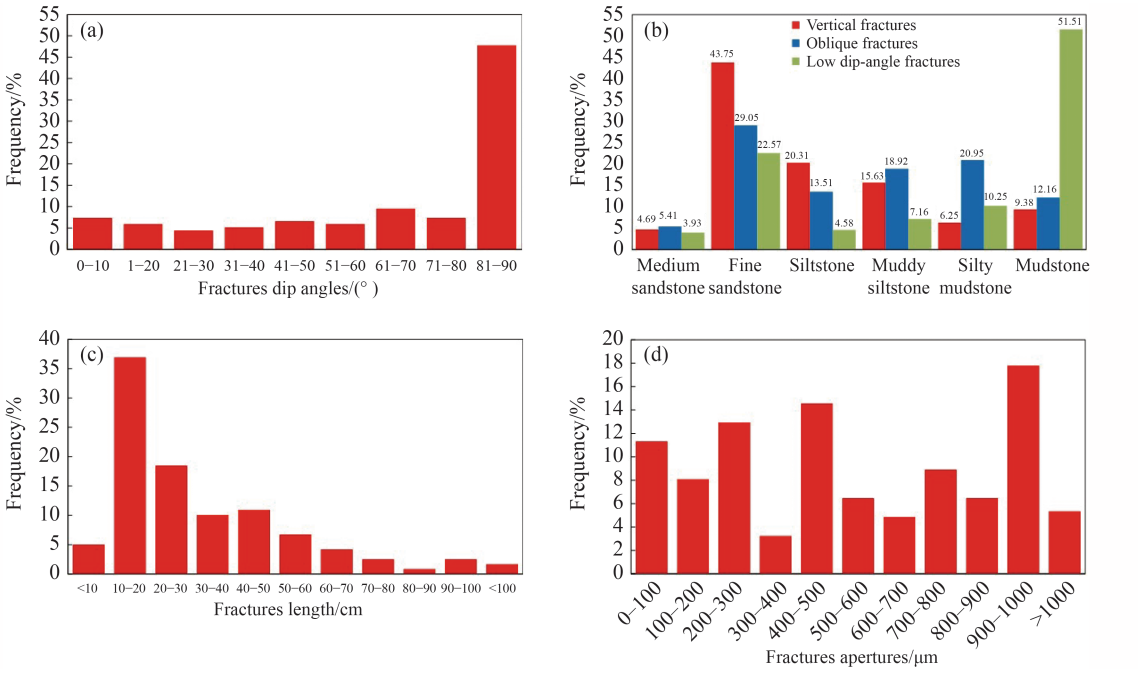


**Fig. 7** Characterization of fractures from cores in the Chang 8 oil-bearing layer of the Upper Triassic Yanchang Formation.

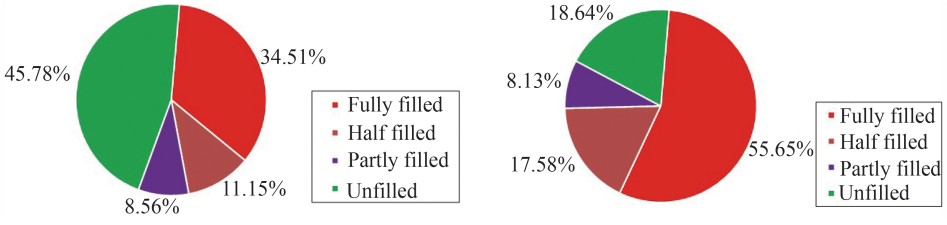


**Fig. 8** Statistics of fracture filling distribution from cores of the Upper Triassic Yanchang Formation. (a) Fractures filled with non-calcareous cementation. (b) Fractures filled with calcareous cementation.

presented as irregular, short, and wormlike curving forms, which are generally filled with crude oil or bitumen (Fig. 9). Overpressure affected the development of the fracture mainly by changing the tectonic stress characteristics of sandstones (Goulty, 2003). The radius of Mohr's circle decreases while the Mohr's circle is to the left, which increases the tangent difficulty of the envelope line to fracture development and makes the transition from shear fractures to tension fractures (Luo et al., 2015). Ordos Basin was a super pressured basin in the geologic history, and the overpressure of the Chang 8 oil-bearing layer member is mainly caused by the hydrocarbon charging from the thick source rocks of the Chang 7 layer. The previous study in Ordos Basin indicates that the overpressure that exists in Chang 8 is caused by the hydrocarbon charging downward from Chang 7 (Luo et al., 2019). The duration of overpressure caused by the charging process matches the main tectonic movements in the Ordos Basin, which indicates that numerous fractures were observed from cores in the Chang 8 oil-bearing layer of the Upper Triassic Yanchang Formation are related to the overpressure.

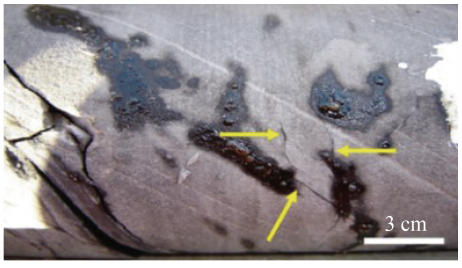


**Fig. 9** Overpressure-related fractures (yellow arrows) presented as wormlike forms in HH16 well (2092.63 m), filled with bitumen.

### 4.4 Micro-scale fractures system

The micro-scale fracture system (developed during tectonic movement and diagenesis-accumulation), whose description is mainly studied by casting thin sections and SEM images. Apertures are critical in micro-scale fractures evaluation. Cmexob (1985) first presented correction methods in the case of micro-fractures not parallel with thin sections. On this basis, micro-fractures apertures can be obtained under the empirical relationship between apertures and hydrostatic pressure (Zeng et al., 2010b).

4.4.1 Fracture types

According to the genetic mechanism, micro-fractures can be also boiled down to tectonic, diagenetic, and overpressure-related categories. 1) Fractures presented regular, narrow, and long strips, and extended with the long axis of deformation minerals or cut through minerals. They are most common from thin sections, accounting for above 72%, which are interpreted as tectonic micro-fractures, whose width is from 5.82 μm to 85.35 μm, with an average of 45.81 μm. Most of the tectonic micro-fractures keep good effectiveness (Figs. 10(a), 10(b), and 10(e)) with a partly filled with 42.1% and unfilled of 11.3%. 2) Fractures have large curvatures and no significant correlation with nearby deformation minerals. These micro-fractures emerged in the veins of sandstones and are filled with bitumen (Figs. 10(c) and 10(f)), which showed obvious overpressure-original characteristics. Overpressure-related micro-fractures ranged from 5.73 μm to 35.07 μm in apertures. 3) Some other micro-fractures are interpreted as diagenetic micro-fractures mainly developed along mineral boundaries or through minerals (Fig. 10(d)). They are greater than tectonic micro-fractures in tortuosity, while less than overpressure-related micro-fractures. Diagenetic micro-fractures are generally filled with minerals such as quartz and calcite, which show poor effectiveness (Fig. 10(d)).

The nanoscale fractures are largely hundreds of tens of nanometers to micrometers in apertures (Fig. 11). Chandler et al. (2013) indicated that nanoscale fractures are more from the secondary process caused by thermochemistry and mechanical processes. Dissolution and diagenesis play a leading role in accelerating the formation of these fractures, and the apertures largely float within micrometers (Fig. 12). For instance, the transformation from montmorillonite to illites and andradite, the existence form of montmorillonite in water stated in hydration state and formed combination with exchangeable cations by hydrogen bond and the water would be released along with the layers under certain pressure and temperature. The fractures between grains caused by the coupling effect of clay minerals dehydration and dissolution are obvious and the average apertures of these nanoscale fractures are about hundreds of nanometers (Figs. 10(g), 10(h), and 10(i)).

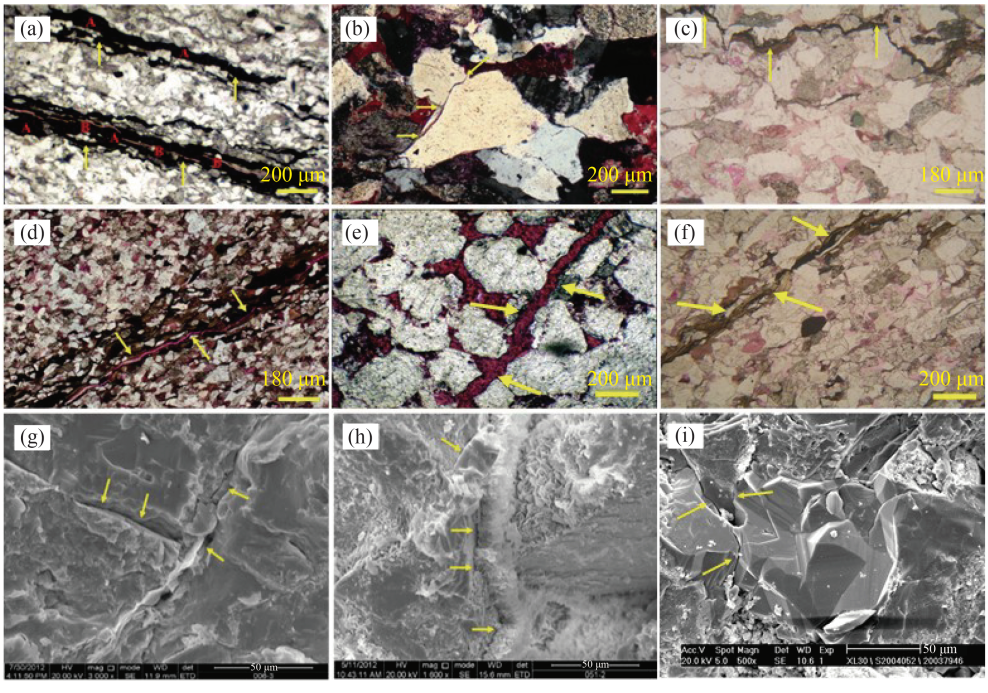


**Fig. 10** Characteristics of micro and nanoscale fractures in the Chang 8 tight sandstones of the Upper Triassic Yanchang Formation. (a) Tectonic micro-fractures (yellow arrows) in a thin section from HH2 well (2062.85 m) under cross-polarized light, partly filled with bitumen and calcite (A-bitumen; B-calcite); (b) open tectonic micro-fractures (yellow arrows) in a thin section from HH39 well (2387.96 m) under cross-polarized light, cutting mineral grains; (c) overpressure-related micro-fracture (yellow arrows) in a thin section from ZJ9 well (2270.79 m) under cross-polarized light, filled with bitumen; (d) diagenetic micro-fracture (yellow arrows) in a thin section from HH9 well (1079.17 m) under cross-polarized light, filled with calcite; (e) open tectonic micro-fractures (yellow arrows) in a thin section without mineral fillings from the ZJ3 well (1586.46 m) under cross-polarized light; (f) overpressure-related micro-fracture (yellow arrows) in a thin section from ZJ17 well (2261.56 m) under cross-polarized light, partly filled with bitumen; (g) nanoscale fracture (yellow arrows) between grains in a SEM image from HH31 well (2196.41 m), partly filled with illite and increases the space by connecting intergranular pores; (h) nanoscale fracture (yellow arrows) and chlorite cladding over grains in a SEM image from HH44 well (2115.17 m); (i) nanoscale fracture (yellow arrows) appears in authigenic quartz particle in a SEM image from HH2 well (2071.41 m).

#### 4.4.2 Fractures characterization

The statistical compilations from casting thin sections revealed that the length of micro-fractures mainly ranged from 0.17 mm to 18.26 mm, with an average of 7.64 mm (Fig. 11(a)). The predominant range of micro-fractures length is 0–10 mm (69.74%) and 15–20 mm (18.42%), with most falling into the range of 0–5 mm (Fig. 11(a)). The width of the micro-fractures was from 0.12 μm to 86.93 μm, and averaged 25.77 μm, with most ranging in 10–20 μm (33.33%) and 20–30 μm (24.44%). Those fractures with a width larger than 50 μm only accounted for 12.22% (Fig. 11(b)). The micro-fractures maintained good effectiveness; whose filling ability depends on the types of micro-fractures.

## 5 Discussion

In multi-scale fracture systems, tectonic fractures have been proven to be the most dominant type controlling "sweet spots". Determination of their formation time and petroleum geological significance will help to understand the contribution of fractures to the formation and distribution of "sweet spots".

### 5.1 The formation time of tectonic fractures

Thirteen calcite-cement samples filled in fractures in tight sandstones are collected for the analysis of isotopes of carbon/oxygen in the Chang 8 sandstones (Liu, 2013). It revealed that the values of $\delta^{18}O_{PDB}$(‰) are from −15.7‰ to −19.7 ‰, mostly distributed in two intervals with −15‰− −18‰ and −18‰− −20‰ (Fig. 12). Supposing the ground surface average temperature is 20°C, the geothermal gradient is 4.5°C/100m, the $\delta^{18}O_{PDB}$( ‰) values corresponding burial depth is from 1114.2 to 2301.8 m. According to the overlapping relationship between burial history and the analysis of carbon/oxygen isotopes, the tectonic fractures in the Chang 8 oil-bearing layer mainly developed during two periods (Fig. 12). The first period is in the Yanshanian Moment, with mainly NWW compressional strike-slip faults and NW shear fractures developed, from the Middle Jurassic to the Late Jurassic (Fig. 13). The second period during the Himalayan Movement, with mainly NEE transtensional strike-slip faults and NE shear fractures developed, was from the beginning of the Paleogene to the end of the Quaternary (Fig. 13).

### 5.2 The petroleum geological significance of multi-scale fractures

The petroleum geological significance of multi-scale fractures is mainly represented in the controlling effect on physical properties (porosity and permeability), development of trap, distribution of oil pools, and production (Table 2).

#### 5.2.1 The effect on controlling trap and accumulation by mega and macro-scale strike-slip fault fracture band

The heterogeneity of mega and macro-scale strike-slip fault fracture bands is manifested by zonation in lateral and segmentation in a strike in the internal structure of the slip fault belt. According to the conceptual model of the internal structure in the slip fault-fractured belt proposed by Torabi et al. (2019), strike-slip fault fracture band laterally consists of a fractured core that accommodates most of the displacement, a damage zone that accompanies fractured core, and wall rocks (Fig. 14).

He et al. (2019) proposed the concept of the fault-fractured body (trap) for the Jinghe Oilfield in the south of Ordos Basin, which is "a reservoir consisting of fractures, associated brittle fractured band, and transformed tight sandstones (wall rock) with non-permeable mudstones and other tight layers as a seal in upper and lateral, such called a fault-fractured body trap."

Chen et al. (2018) systematically analyzed fluid inclusions in the quartz and calcite-cemented tight sandstones tectonic fractures from the Chang 8 sandstones. These inclusions assemblages are distributed as banding, and the diameter of most assemblages ranges from 5 to 10 μm. The homogenization temperatures of fluid inclusions assemblages represented by the secondary concrescence of quartz edge and microfractures are from 46°C to

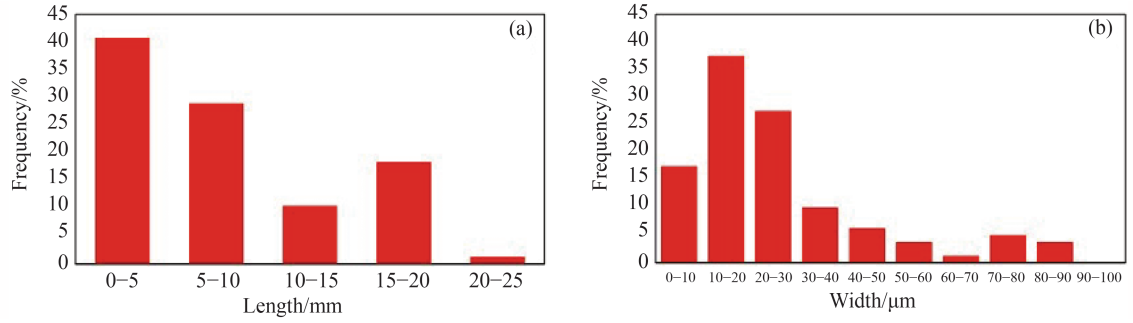


**Fig. 11** The micro-fractures characteristic from thin sections of the Chang 8 sandstones. (a) Micro-fractures length. (b) Micro-fractures width.

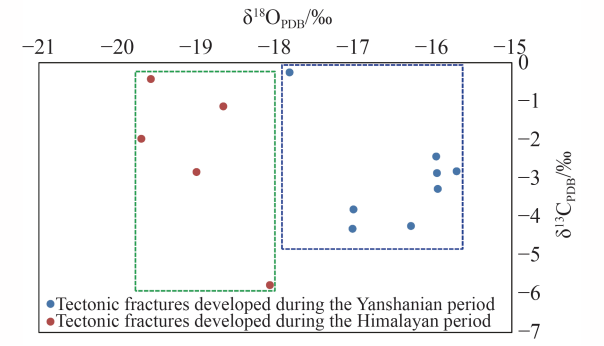


**Fig. 12** The result of carbon/oxygen isotopes analysis in the fractures with mineral-filled of the Chang 8 tight sandstones. The data of carbon/oxygen isotope samples in the quartz and calcite-cemented were from Chen et al. (2018), and the carbon/oxygen isotope data were used to calculate the fractures formation temperature based on the temperature measurement equation. The fractures formation periods were deduced by correspondence between fractures formation depth and burial depth based on fractures formation temperature and geothermal gradients from Liu (2013).

143°C, and homogenization temperatures of calcite fluid inclusions assemblages are from 100°C to 115°C. According to the burial history (Fig. 13), the Chang 8 oil-bearing layer is mainly characterized as three periods of charging and accumulation from the source rocks of Chang 7 (Wang et al., 2017a).

The first period was during the middle-late Jurassic with fluid-inclusion homogenization temperatures from 60°C to 90°C, where early hydrocarbon recharging developed. The second period was at the end of the Jurassic to the middle Cretaceous with fluid-inclusion homogenization temperatures from 90°C to 125°C, where middle hydrocarbon charging developed. The third period, with fluid-inclusion homogenization temperatures from 125°C to 150°C, was from the middle Cretaceous to the Early Paleogene, where late hydrocarbon charging developed. As discussed above, the meso-scale tectonic fractures are the main fluid flow pathways in Chang 8 tight sandstones, and the tectonic micro-fractures improve the seepage capability by connecting intergranular pores

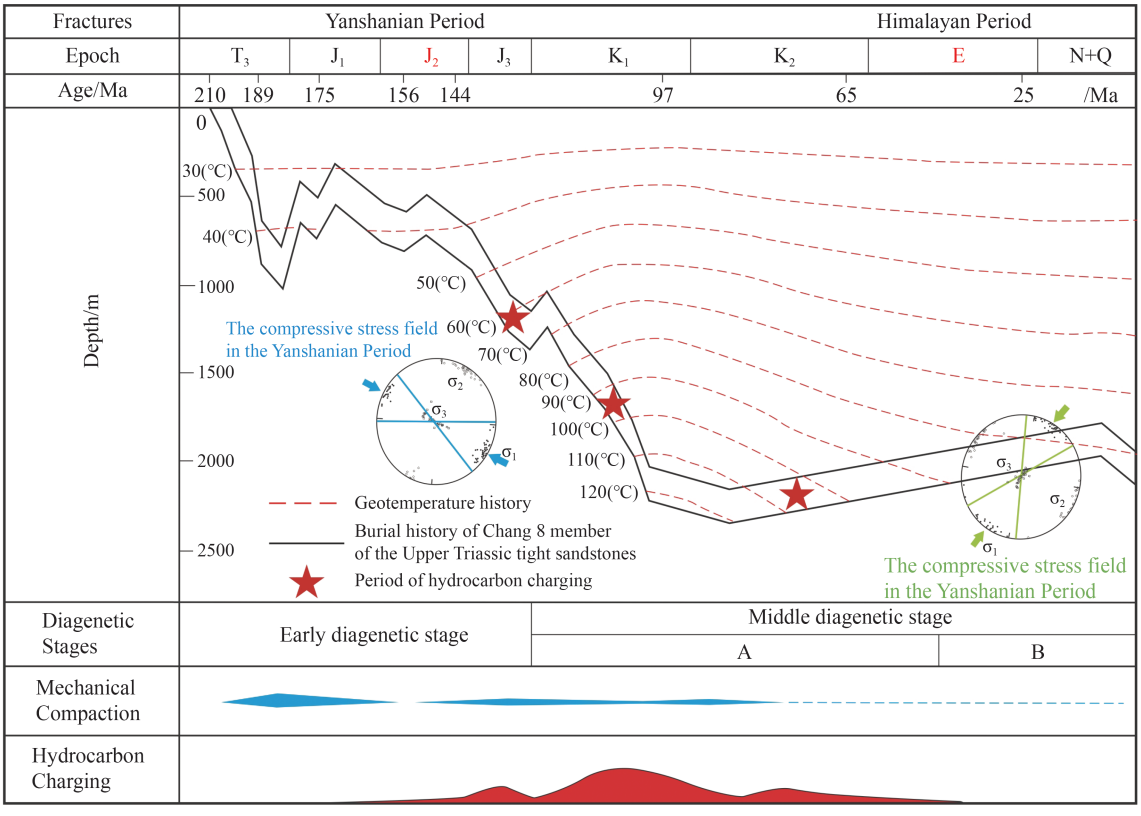


**Fig. 13** Geotemperature history, burial history, and fluid-inclusion homogenization temperature of calcite and quartz deposits in tectonic fractures in the Chang 8 tight sandstones, south-western Ordos Basin. The burial history was derived from the stepwise stratigraphic back-stripping technique according to compaction correlation, regional denudation data from Wang et al. (2017b). The data of temperature was from Bai (2013). The fluid inclusions data of the calcite and quartz deposits in the tight gas sandstones of the Chang 8 oil-bearing layer of the Upper Triassic Yanchang Formation were from Chen et al. (2018). The "$J_2$" is the first period of fractures development in the Yanshannian Period, and the "E" is the second period of fractures development is in the Himalayan Period. (a) The first hydrocarbon charging period with fluid-inclusion homogenization temperatures from 60°C to 90°C in the middle-late Jurassic. (b) The second hydrocarbon charging period with fluid-inclusion homogenization temperatures from 90°C to 125°C, was from the end of the Jurassic to the middle Cretaceous. (c) The third hydrocarbon charging period with fluid-inclusion homogenization temperatures from 125°C to 150°C, was from the middle Cretaceous to the Early Paleogene. T-Triassic; J-Jurassic; K-Cretaceous; E-Eogene; N-Neogene; Q-Quaternary.

**Table 2** Characteristics of multi-scale fractures in the Chang 8 tight sandstones

| Category | Scale | Length /mm | Morphology | Extension | Characterization methods | Origin | Geological significance |
|---|---|---|---|---|---|---|---|
| Ⅰ | Mega-scale | $>7\times10^7$ | NWW strike-slip faults | Cutting through some geological stratums | Seismic data and outcrops | Tectonic movement | Cutting across Chang7 source rocks and Chang 8 sand layers, acting as pathways for hydrocarbon charging down, and controlling the oil accumulation and forming fault-fracture body trop |
| Ⅱ | Macro-scale | $3.5\times10^5$–$7\times10^7$ | NWW strike-slip faults and fractures | | | | |
| Ⅲ | Meso-scale | 10–$3.5\times10^3$ | Fold-shaped diagenetic fractures. Wormlike over pressure related fractures.NW,NE,SN and EW fractures with NE and NW fractures as priority | Sand body controlled | well logs (conventional and image well logs and cores) | Tectonic movements, diagenesis, and overpressure | Increasing porosity, permeability, flow ability and production |
| Ⅳ | Micro-scale | <10 | Develope as the shape of diagenetic minerals | Mineral grains and diagenesis controlled | Casting thin sections, SEM images and micro-CT | | |

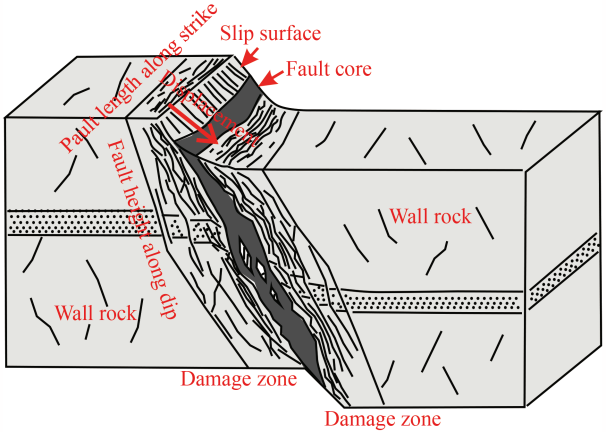


**Fig. 14** The conceptual model of strike-slip fault band (Torabi et al., 2019).

and intergranular pores. Overpressure-related fractures, serving as storage space and enhancing seepage capability, developed during hydrocarbon charging.

The extension length of the mega and macro-scale strike-slip fault-fracture system is large enough to cut through the Chang 8 tight sandstones and extend to the upper Chang 7 source rocks, and a fault-fractured body trap developed for effective communication, which enables the hydrocarbon generated in Chang 7 source rocks to charge and accumulate through the mega-scale longitudinal fault-fracture system.

For petroleum exploration and development, it has been proved that hydrocarbon accumulations are particularly affected by the fault-fractured body trap controlled by the strike-slip faults in the Chang 8 Member of the Honghe Oilfield. Figure 15 is the map of the distribution of multi-scale fracture bands and oil saturation in tight sandstones around the fractured band. The fault-fractured body trap and hydrocarbon distribution in fault-fractured body reservoirs are significantly influenced by the mega-scale NW fault bands and the macro-scale NE fault bands. The later tectonic movements are much stronger in the NE than that in the NW, resulting in better oil-bearing properties around the NE fault band (Fig. 15).

### 5.2.2 The effect on controlling physical properties and production of tight sandstone by meso and micro-scale fractures

#### 5.2.2.1 The effect on controlling physical properties of tight sandstone by meso-scale fractures

The most important effect of fractures on physical properties is reflected in the change in permeability, followed by the increase in porosity (Ougier-Simonin et al., 2016). By using the Monte Carlo method and fractures geometry evaluation system, the porosity and permeability of fractures can be calculated from cores, sections, and SEM observations. The porosity of micro-fractures is 0.51%–2.49%, and the permeability is 0.09–23.90 md. The porosity of high dip-angle (including vertical) tectonic shear fractures is 1.22%–2.51%, and the permeability is 4.47–23.90 md with an average of 10.87 md. The porosity of low dip-angle tectonic shear fractures is 0.61%–1.41%, and permeability is 0.24–4.85 md. The porosity of horizontal tectonic shear fractures is 0.92%–1.65%, and permeability is 1.06–3.36 md (Fig. 16).

The matrix porosity and permeability were 1%–15% and 0.01–1 md, respectively. The contribution of macro-fractures to porosity is limited, however, the average macro-fractures permeability, especially those of high dip-angle tectonic shear fractures is 9–23.9 times that of the matrix. The vertical overpressure-related and tectonic extension fractures represent small fractions of total fractures, and the effect on reservoir porosity is not as good as tectonic fractures. High dip-angle tectonic shear fractures cut through sand bodies and connect fractures networks, providing effective spaces for hydrocarbon charging and primary seepage pathways.

The physical properties contribution of micro and nano scale fractures are smaller, and tectonic micro-fractures

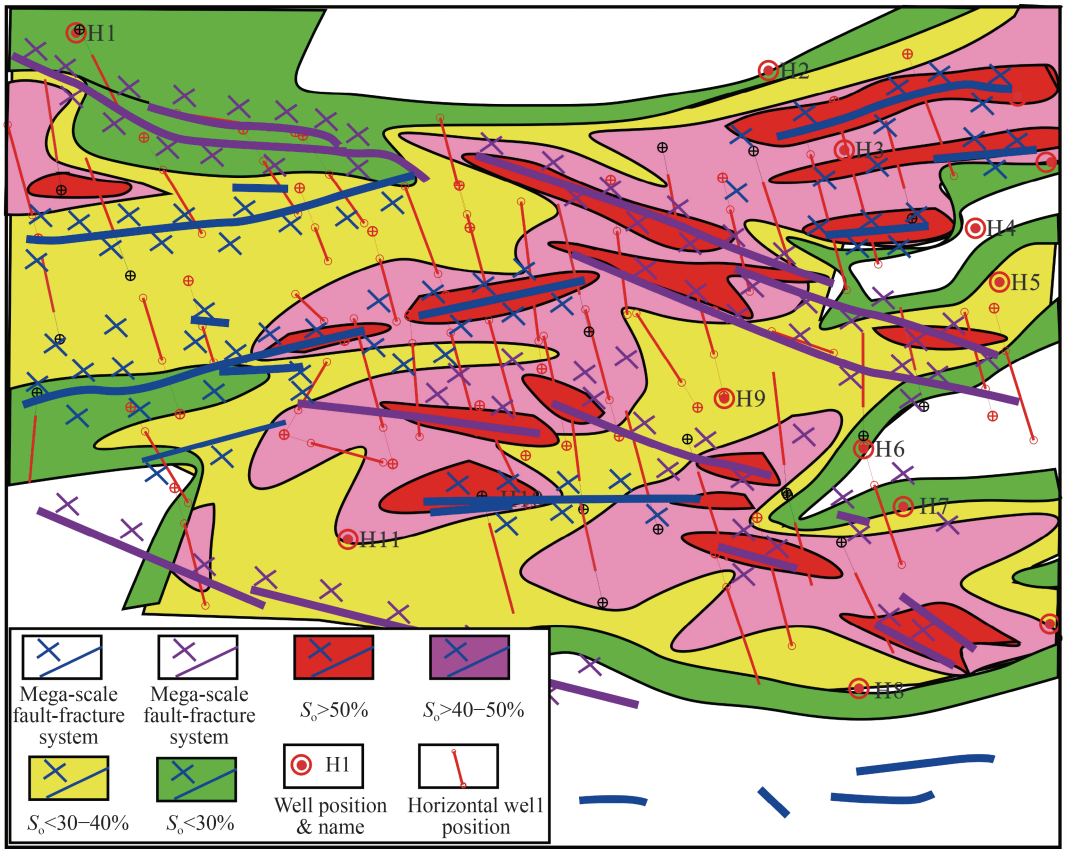


**Fig. 15** Distribution of multi-scale fracture band and the oil saturation of tight sandstones.

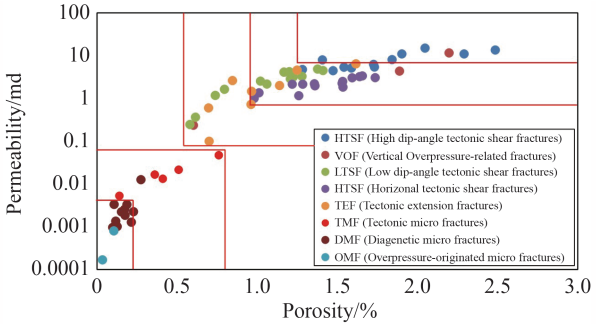


**Fig. 16** The distribution diagram of fractures porosity and permeability. The fractures porosity and permeability were calculated by the Monte Carlo method from cores, casting thin sections, and SEM images observations.

with an average porosity of 0.42% and average permeability of 0.019 md are mostly contributed, followed by diagenetic fractures and overpressure-related fractures, whose average porosity and permeability is less than 0.16%, 0.01 md and 0.1%, 0.01 md, respectively (Fig. 16). The average porosity and permeability of tectonic micro-fractures are approximately 8% and 20% of average matrix porosity and permeability. Diagenetic and overpressure-related micro-fractures are less abundant compared with tectonic micro-fractures, and their average porosity and permeability are much smaller than matrix, whose improvement to reservoirs' physical properties is barely ineffective. Tectonic micro-fractures generally developed with the boundary and cutting through grains (Fig. 10).

#### 5.2.2.2 The effect on controlling production by micro-scale fractures

The Chang 8 tight sandstones mainly developed high dip-angle and vertical tectonic fractures according to core observation, whose development is controlled by the distance to faults. The ends and sides of faults are superior areas for tectonic fractures development, the influence distance of faults to fractures is about 2–4 km (Fig. 17).

Under the influence of the present stress field with NE-SW trending in the Honghe oil field, the NEE faults and fractures keep their openness well, which have better conductivity. While the NWW faults and fractured band presented as compress-torsional faults with poor conductivity and effectiveness. The NEE faults and fractured band are tensional-torsional. Therefore, the wells drilled in the NWW fractured band represented as low-yield with an average of 1.32 t/d (Fig. 18), however, the wells drilled in the NEE fractured band represented as better-yield is about 8–15 t/d in production capacity with an average of 9.32 t/d (Fig. 18), high-yield wells (> 9 t/d) distributed mainly in the intersection area of NWW and NEE fractured regions (Fig. 18).

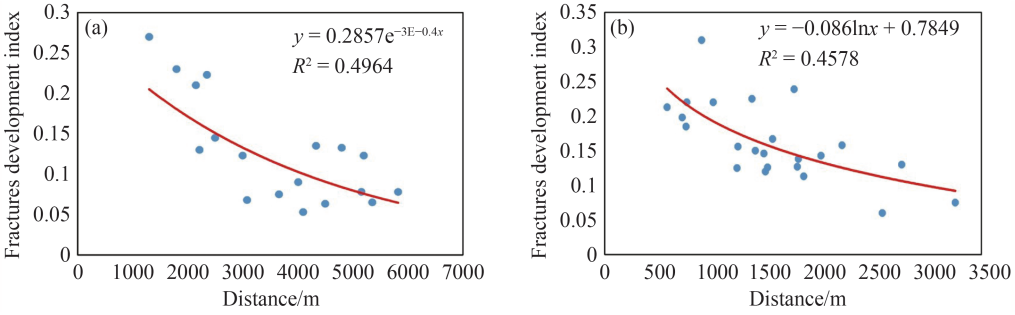


**Fig. 17** The scatter plot of fractures development index from well logs (the ratio of fractured layers thickness to statistical subzone thickness) and distance of fractures to faults in the fault number one and number two.

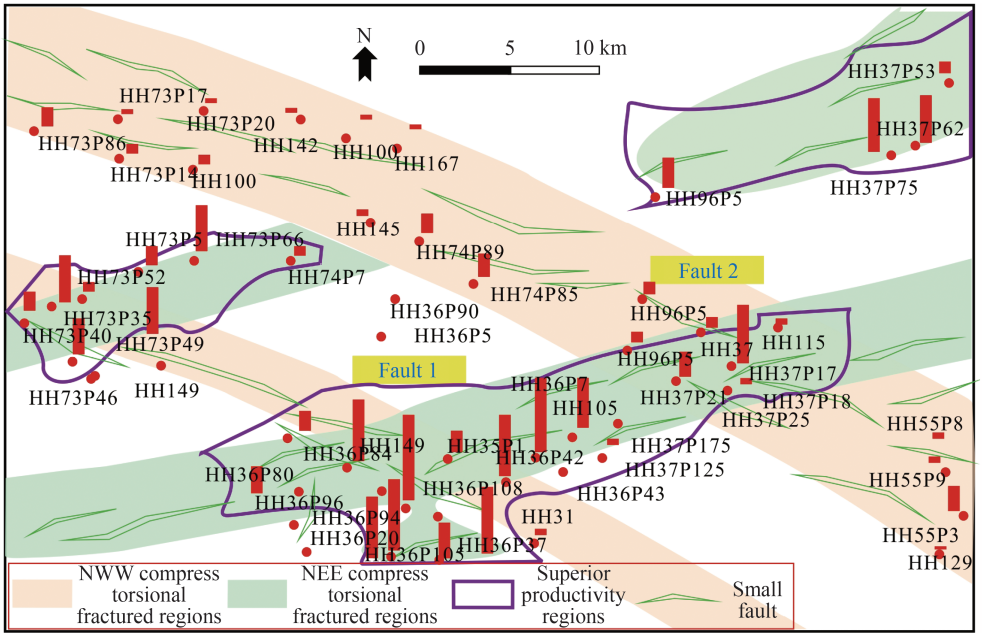


**Fig. 18** Production capacity distribution sketch map in different faults and fractured regions. The production capacity in NEE and NNE fractured regions is significantly better than the production capacity in NNW fractured region, and the high-yield wells (> 9 t/d) are distributed mainly in the intersection area of NWW, NNE and NEE fractured regions.

## 6 Conclusions

Comprehensive characterization and analysis of natural fractures in Chang 8 tight sandstone reservoirs leads to the following conclusions.

1) Four scales, three periods of strike-slip faults, and associated fracture systems are mainly developed in the Chang 8 tight sandstones of the Honghe Oilfield: mega and macro-scale strike-slip faults developed during the Middle-Late Triassic, mainly accompanied by four groups of fractures (NW, NNE, NE, and EW) representing large shear fractures associated with Yanshannian (left-rotation) and Himalayan (right-rotation) Tectonic Movements, respectively. The macro-scale fractures are mainly NE slip fault zone developed in the Middle Jurassic Yanshannian Period. The meso-scale fractures system are mainly tectonic fractures and developed during the Himalayan Period. The micro-scale fracture system is mainly developed during tectonic movement and diagenesis-accumulation.

2) The NWW faults and NW tectonic shear fractures developed during the Yanshannian Tectonic Movement, which is from the Middle Jurassic to the Late Jurassic, and the NEE faults and NE tectonic shear fractures developed during the Himalayan Tectonic Movement, which is from the beginning of the Paleogene to the end of the Quaternary. Meanwhile, hydrocarbon-charging is late than the first period of tectonic fractures but early than the second period of tectonic fractures. The first period of tectonic fractures provided storage spaces for the subsequent charging, and the second period of tectonic fractures adjusted the hydrocarbon accumulation and distribution.

3) Mega and macro-scale strike-slip faults are characterized by strike-segmentation and lateral zonation, and longitudinally communicate with source rocks and have the characteristics of controlling trap and reservoirs; the fault-fractured body traps controlled by strike-slip fracture band are critical to hydrocarbon accumulation

and reservoir development; the late NE tectonic fractures (macro-scale) are mainly tensional with strong movement, resulting in better oil-bearing properties in the NE direction than in the NW fractures (mega-scale).

4) Horizontal tectonic shear fractures, extension fractures, and diagenesis shrinkage fractures in meso-scale could increase the connectivity of sand bodies and play as storage spaces. Tectonic micro-fractures were more of throats with adjacent pores and could improve the permeability. Diagenetic micro-fractures generally present as filled minerals and are negligible for the improvements in physical properties. Overpressure-related micro-fractures are generally filled with crude oil or bitumen. The contribution of this scale of fractures to reservoirs' physical properties is mainly reflected in permeability improvement, while the contribution to storage spaces is relatively weak.

5) The high-yield wells are mainly distributed in the intersection area of NWW and NEE fractured regions, followed by the wells along the NEE transtensional strike-slip faults and NE shear fractures, low-yield wells with mainly distributed along the NWW fractured zones or drilled with NW fractures.

**Acknowledgments** We thank the financial support from the National Natural Science Foundation of China (Nos. 41902147 and 41402117) and the China National Science and Technology Major Project (No. 2016ZX05048-001–01-CS). We also thank the Sinopec Huabei Company for providing the core samples and the other data sets, and the permission to publish this article.

## References

Bai B, Zou C, Zhu R, Zhang J, Tan J, Zhang B, Yang H, Cui J, An X (2012). Characteristics and Formation stage-times of structural fractures in tight sandstone reservoir of the 2nd Member of Xujiahe Formation in southwestern Sichuan Basin. Acta Geol Sin, 86(11): 1841–1846

Bai Y (2013). The coupling mechanism of the diagenetic evolution and oil accumulation process of Chang-7 tight sandstone reservoir in Wubao area, Ordos Basin. The Dissertation for Doctoral Degree. Xi'an: Northwest University

Baytok S, Pranter M J (2013). Fault and fracture distribution within a tight-gas sandstone reservoir: Mesaverde Group, Mamm Creek Field, Piceance Basin, Colorado, USA. Petrol Geosci, 19(3): 203–222

Chandler M R, Meredith P G, Crawford B R (2013). Experimental determination of the fracture toughness and ductility of the Mancos Shale. In: 75th EAGE Conference & Exhibition Incorporating SPE EUROPEC 2013, Utah

Chen H, Zhu X, Chen C, Yi W, Shi R (2018). The coupling relationship of reservoir densification history and hydrocarbon emplacement in tight sandstone reservoir: a case study of the Chang 8 Oil Member, Yanchang Formation, southern Ordos Basin. Acta Sediment Sin, 36(02): 401–414

Cmexob E M (1985). Fundamental Theory and Method of Fractured Reservoir Exploration. Beijing: Petroleum Industry Press (in Chinese)

Dai J, He S (2010). Discovery and significance of faults in the Mid Gasfield, Ordos Basin. Pet Explor Dev, 37: 188–195

Deng X, Luo A, Zhang Z, Liu X (2013). Geochronological comparison on Indosinian tectonic events between Qinling Orogeny and Ordos Basin. Acta Sediment Sin, 31(6): 939–953

Derikvand B, Alavi S A, Fard I A, Jalali L (2019). Changing in fold geometry from faulted detachment fold to fault-bend fold, a case study: the Zeloi Anticline in the Dezful Embayment, southwest of Iran. J Petrol Sci Eng, 173: 381–401

Duan Y, Wang C Y, Zheng C Y, Wu B X, Zheng G D (2008). Geochemical study of crude oils from the Xifeng Oilfield of the Ordos Basin, China. J Asian Earth Sci, 31(4−6): 341–356

Ding W, Zhu D, Cai J, Gong M, Chen F (2013). Analysis of the developmental characteristics and major regulating factors of fractures in marine-continental transitional shale-gas reservoirs: a case study of the Carboniferous−Permian strata in the southeastern Ordos Basin, central China. Mar Pet Geol, 45: 121–133

Goulty N R (2003). Reservoir stress path during depletion of Norwegian chalk oilfields. Petrol Geosci, 9(3): 233–241

Han W, Zhao X, Pu X, Chen S, Wang H, Liu Y, Shi Z, Zhang W, Wu J (2021). Fine-grained rock fabric facies classification and its control on shale oil accumulation: a case study from the Paleogene Kong 2 Member, Bohai Bay Basin. Front Earth Sci, 15(2): 423–437

He F Q, Liang C C, Lu C, Yuan C Y, Li X W (2019). Identification and description of fault-fracture bodies in tight and low permeability reservoirs in transitional zone at the south margin of Ordos Basin. Oil Gas Geol, 41(4): 710–718

Jiang L, Wang Q C, Wang X Z, Jiang C F, Zhang L X, Xue Z H, Chu Y (2013). Joint development and paleostress field in Mesozoic strata of the southeastern Ordos Basin. Acta Petrol Sin, 29(5): 1774–1790

Ju W, Niu X, Feng S, You Y, Xu K, Wang G, Xu H (2020). Present-day *in-situ* stress field within the Yanchang Formation tight oil reservoir of Ordos Basin, central China. J Petrol Sci Eng, 187: 106809

Li Y, Gao X, Meng S, Wu P, Niu X, Qiao P, Elsworth D (2019a). Diagenetic sequences of continuously deposited tight sandstones in various environments: a case study from upper Paleozoic sandstones in the Linxing area, eastern Ordos Basin, China. AAPG Bull, 103(11): 2757–2783

Li Y, Yang J, Pan Z, Meng S, Wang K, Niu X (2019b). Unconventional natural gas accumulations in stacked deposits: a discussion of Upper Paleozoic coal-bearing strata in the east margin of the Ordos Basin, China. Acta Geol Sin, 93(1): 111–129

Li Y, Tang D, Wu P, Niu X, Wang K, Qiao P, Wang Z (2016). Continuous unconventional natural gas accumulations of Carboniferous−Permian coal-bearing strata in the Linxing area, northeastern Ordos Basin, China. J Nat Gas Sci Eng, 36: 314–327

Liu Y (2013). Fracture characteristics of low permeability reservoirs and the control action of the accumulation of oil and gas—a case study of Member Chang 8 in the Red River Oilfield. Dissertation for the Doctoral Degree. Chengdu: Chengdu University of Technology

Liu Z, Yao X, Hu X D, Xia L, Wang J (2013). Discovery of the Middlezoic fault and its implication on the hydrocarbon accumulation in Ordos Basin. J Earth Sci Environ, 35(02): 56–66

Luo C, Jia A, Guo J, Tian Q, Wang J, Lin H, Yin N, Gao X (2021). A quantitative study of the scale and distribution of tight gas reservoirs in the Sulige Gas Field, Ordos Basin, northwest China. Front Earth Sci, 15(2): 457–470

Luo Y, Wang Y, Liu H, Wang G, Zhao Y (2019). Overpressure controlling factors for tectonic fractures in near-source tight reservoirs in the southwest Ordos Basin, China. J Petrol Sci Eng, 496: 106818

Luo Y, Zhao Y, Chen H, Su H (2015). Fracture characteristics under the coupling effect of tectonic stress and fluid pressure: a case study of the fractured shale oil reservoir in Liutun subsag, Dongpu Sag, Bohai Bay Basin, eastern China. Pet Explor Dev, 42(2): 196–205

Nelson R A, Moldovanyi E P, Matcek C C, Azpiritxaga I, Bueno E (2000). Production characteristics of the fractured reservoirs of the La Paz Field, Maracaibo Basin, Venezuela. AAPG Bull, 84(11): 1791–1809

Olson J E, Laubach S E, Lander R H (2009). Natural fracture characterization in tight gas sandstones: integrating mechanics and diagenesis. AAPG Bull, 93(11): 1535–1549

Ougier-Simonin A, Renard F, Boehm C, Vidal-Gilbert S (2016). Microfracturing and microporosity in shales. Earth Sci Rev, 162: 198–226

Pan X, Zhou L F, Liu B H, He X, Liu W G (2010). Study on fractures of outcrop area in Lower Cretaceous in central and western Ordos Basin. Fault-Block Oil Gas Field, 17(4): 430–433

Torabi A, Ellingsen T S S, Johannessen M U, Alaei B, Rotevatn A, Chiarella D (2019). Fault zone architecture and its scaling laws: where does the damage zone start and stop? Geol Soc London Sp Public, 496(1): SP496–2018-151

Wang C Y, Zheng R C, LI Z Q, Wang H H, Xin H G, Liang X W (2010). Characteristics of lithologic reservoir of interval 8 of Yanchang Formation in Jiyuan Oilfield of Ordos Basin. Geol Sci Tech Inform, 29(3): 69–74

Wang F, Yi W, Chen C (2017a). Genetic mechanism of sweet spot of tight sandstone reservoirs in Chang 8 Layer of Honghe Oil Field, Ordos Basin. Petrol Geo Exper, 39(04): 484–490

Wang G, Chang X, Yin W, Li Y, Song T (2017b). Impact of diagenesis on reservoir quality and heterogeneity of the upper Triassic Chang 8 tight oil sandstones in the Zhenjing area, Ordos Basin, China. Mar Pet Geol, 83: 84–96

Wang Y, Liu L, Li S, Ji H, Xu Z, Luo Z, Xu T, Li L (2017c). The forming mechanism and process of tight oil sand reservoirs: a case study of Chang 8 oil layers of the Upper Triassic Yanchang Formation in the western Jiyuan area of the Ordos Basin, China. J Petrol Sci Eng, 158: 29–46

Yao J L, Zhao Y D, Liu G L, Qi Y L, Li Y H, Luo X A, Zhang X L (2018). Formation patterns of Chang 9 oil reservoir in Triassic Yanchang Formation, Ordos Basin, NW China. Pet Explor Dev, 45(3): 389–401

Zeng L, Jiang J, Yang Y (2010a). Fractures in the low porosity and ultra-low permeability glutenite reservoirs: a case study of the late Eocene Hetaoyuan formation in the Anpeng Oilfield, Nanxiang Basin, China. Mar Pet Geol, 27(7): 1642–1650

Zeng L, Su H, Tang X, Peng Y, Gong L (2013). Fractured tight sandstone oil and gas reservoirs: a new play type in the Dongpu depression, Bohai Bay Basin, China. AAPG Bull, 97(3): 363–377

Zeng L B, Ke S Z, Liu Y (2010b). Fracture Study Methods for Low Permeability Oil and Gas Reservoir. Beijing: Petroleum Industry Press (in Chinese)

Zhang M Z, Ji L M, Wu Y D, He C (2015). Palynofacies and geochemical analysis of the Triassic Yanchang Formation, Ordos Basin: implications for hydrocarbon generation potential and the paleoenvironment of continental source rocks. Int J Coal Geol, 152(12): 159–176

Zou C, Yang Z, Tao S, Yuan X, Zhu R, Hou L, Wu S, Sun L, Zhang G, Bai B, Wang L, Gao X, Pang Z (2013). Continuous hydrocarbon accumulation over a large area as a distinguishing characteristic of unconventional petroleum: the Ordos Basin, north central China. Earth Sci Rev, 126: 358–369